Materials Research. 2022; 25:e20220129
DOI: https://doi.org/10.1590/1980-5373-MR-2022-0129

Assessment of Charge Transport Through Barrier Membranes Before Application on Materials Surfaces

***Jéssica Verger Nardeli*[a]*, *Cecílio Sadao Fugivara*[a], *Assis Vicente Benedetti*[a]**

[a]*Universidade Estadual Paulista, Instituto de Química, Araraquara, SP, Brasil.*

Received: March 15, 2022; Revised: July 6, 2022; Accepted: August 21, 2022.

This work aims at investigating the charge transfer resistance (R_{CT}) of the two membranes derived from vegetable oils which are intended to protect materials against corrosion. The membranes were characterized by thickness measurement (328±1 µm and 491± 1 µm), atomic force microscopy (AFM) to estimate of roughness (<0.5 µm), Raman spectroscopy while the R_{CT} values were evaluated by electrochemical impedance spectroscopy (EIS) in 0.1 mol/L KCl solution. EIS was used to measure the impedance at low frequency ($Z_{0.01Hz} \cong 10^9\ \Omega\ cm^2$), $R_{CT} \cong 10^9\ \Omega\ cm^2$ and exchange current density ($i_0 \cong 10^{-11}\ \Omega\ cm^2$), employing simple instrumentation. The thickness of the membrane must be considered for coherent interpretation of the impedance results. The study of electrolytes permeation in membranes is important to previously estimate the lifetime offered to a substrate over the time of immersion even before being applied to the metallic surface. The impedance measurements demonstrated that the most resistant membrane to permeation presented a R_{CT} around 2 GΩ cm^2. This EIS measurements approach enables the optimization of membrane fabrication by conveniently identifying the best formulation.

Keywords: *Membrane, pristine organic film, permeation, corrosion protection.*

Graphical abstract

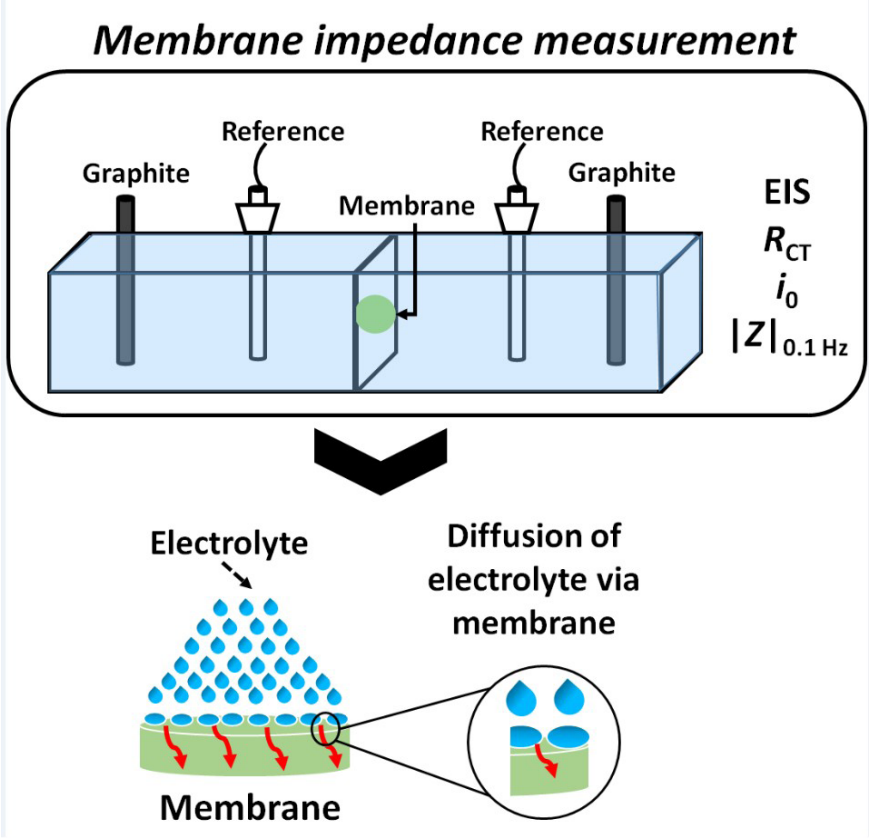

*e-mail: jeh.nardeli@gmail.com

1. Introduction

The development of protective coatings based on new materials with self-healing properties has been a route to obtain efficiency in the protection of some substrates against corrosion. Many papers were devoted to the development of coatings / films for protection materials against corrosion or degradation[1-11] however, no one of them report on studies of the evaluation of the charge transfer resistance (R_{CT}) during the electrolyte permeation through the pristine film.

Some studies have shown that EIS is a valuable tool for membrane characterization[12-16]. EIS is a non-destructive technique[17] that can provide information about electrochemical phenomena including permeation processes. These studies expanded the scope of membrane functionality and analysis and, moreover, highlight the opportunity for investigation prior to membrane utilization / application.

A few studies[18-20] have used a permeation cell to investigate the permeation of K^+ ions through membranes measuring their R_{CT} values with immersion time. The study of ions permeation through the free film extends to different systems as described in the literature[21,22].

This study can also be applied as a previous investigation of film barrier properties in the development of new coatings for metallic protection against corrosion, constituting in a selective process of these materials. Therefore, it is of great interest to estimate the barrier properties, stability, and durability of barrier effect of organic membranes, and organic inorganic hybrid materials before applying on a metallic substrate to protect it against corrosion.

In this context, the purpose of this work is to develop and characterize organic free membranes, by measuring the thickness, roughness using atomic force microscopy (AFM), chemical constitution with Raman spectroscopy and to estimate the barrier property by electrochemical impedance spectroscopy during immersion in 0.1 mol/L KCl solution. From the electrochemical measurements in a permeation cell, it is possible to obtain several parameters correlated to the membrane properties, i.e., R_{CT}, exchange current density (i_0), and low frequency impedance ($|Z|_{0.01Hz}$) that allow accessing the barrier properties of the membranes and predicting their performance when applied as coatings. The performance of the free membranes will be compared with the corresponding coatings already applied on aluminum alloys[1].

2. Materials and Methods

2.1. Materials

Castor oil (CAO) was purchased from Asher® and crambe oil (CO) provided by Foundation Mato Grosso do Sul. Trimethylolpropane (TMP), phthalic anhydride (PhA), butylated hydroxyl toluene (BHT), propyl glycol (PG), butyl acetate (BA), ethyl glycol acetate (EGA), hexamethylene diisocyanate (HDI), lithium hydroxide (LiOH), n-butyl acetate (BA), ethyl glycol acetate (EGA) and stannous octoate (SO) were all acquired commercially and used as received.

2.2. Preparation of membranes (pristine membranes)

Two membranes, herein denominated membrane **A** and membrane **B**, were prepared as the procedure shown in Scheme 1.

Firstly, polyester (Scheme 1a) was synthesized according to our previous works[23,24] through the reaction of CO (1 mol), TMP (5 mols), PhA (3 mols), BHT (0.005 mol), LiOH (0.0104 mol) at 240 °C for 5 h, N_2 atmosphere, under stirring. Secondly, prepolymer (Scheme 1b) was synthesized through the reaction of CAO (0.214 mol), TMP (0.178 mol), BHT (0.005 mol), PG (0.084 mol), BA (1.918 mols), EGA (0.725 mol), HDI (1.555 mols) at 60 °C for 6 h, N_2 atmosphere, under stirring. Then the membranes (Scheme 1c, d) were formulated: Membrane **A** (Scheme 1c) through the reaction of polyester (1 mol), prepolymer (3 mols), SO catalyst ($3.45x10^{-4}$ mol) at 25 °C for 10 min, under stirring and Membrane **B** (Scheme 1d) through the reaction of polyester (1 mol), prepolymer (2 mols), SO catalyst ($3.45x10^{-4}$ mol) at 25 °C for 10 min, under stirring.

The experimental procedure for obtaining the free membranes is illustrated in Figure 1. Teflon was used as a substrate because membranes are easy removed without causing damage to the surface. The substrate was washed with deionized water and stored in a closed environment at 25 °C. After the preparation of the membranes **A** and **B**, they were applied on the substrate surface with the aid of an extensometer and maintained at 25 °C for 48 h. Then, the membranes were removed from the Teflon surface and stored in a desiccator until the characterization experiments were started.

2.3. Thickness of the membranes

The average thickness of the membranes (eight measures each sample) was determined with a MITUTOYO micrometer

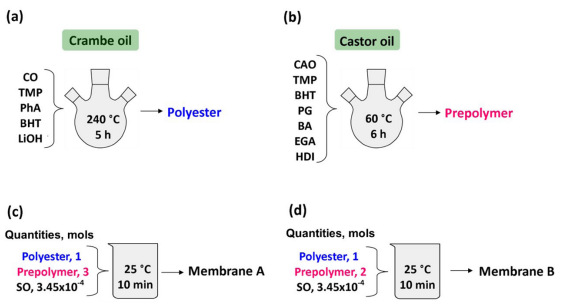

Scheme 1. (a, b) Modification of vegetable oils and (c, d) formulation of membranes.

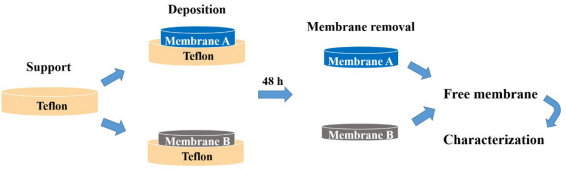

Figure 1. Scheme to obtain the free membranes **A** and **B**.

0-25 mm/0.01 mm in different regions of the membrane to evaluate homogeneity of thickness throughout the film length.

2.4. Atomic Force Microscopy (AFM)

The membranes before and during 1, 4 and 24 h of immersion in 0.1 mol/L KCl solution were analyzed in situ by phase images obtained with an atomic force microscope, acquired in tapping mode with a scan size of 5 × 5 μm^2 and from 2 × 10^5 Hz to 4 × 10^5 Hz frequency range. The treatment of AFM images was made using the Gwyddion® software.

2.5. Raman spectroscopy

The membranes before and after 7 days of immersion in 0.1 mol/L KCl solution were analyzed by Raman spectroscopy using a Fourier transform Raman spectrometer (Bruker's RAMII model) at 1064 nm wavelength with a laser power of 100 mW as the radiation source with acquisition time of 6 min. The special difference is the polyester / prepolymer ratio. For each Raman spectrum 200 scans were performed in the range of 4000 - 500 cm^{-1} with a resolution of 4 cm^{-1}.

2.6. Electrochemical impedance spectroscopy (EIS) of the membrane in the permeation cell

Figure 2 shows a scheme of the permeation cell used in the $R_{CT,}$ i_0 and $|Z|_{0.01Hz}$ measurements[18-22]. The permeation cell was constructed in our laboratory[26] based on the Devanathan-Stachurski cell[25] containing two compartments to place four electrodes to the impedance measurements, operating with 50 mL of electrolyte in each compartment. Each compartment contained two electrodes: compartment 1- (a) working electrode: graphite stick; (b) reference electrode (work sense): reference electrode Ag|AgCl|KCl (3mol/L); compartment 2- (d) reference electrode: Ag|AgCl|KCl (3mol/L); (e) counter electrode: graphite stick and (c) the intersection between the two compartments of the cell, separated by the membrane to be studied, whose exposed area to the electrolyte was 1 cm^2.

The measurements were carried out in a GAMRY REFERENCE 600 potentiostat-galvanostat. The aqueous solution was 0.1 mol/L KCl because both K^+ and Cl^- ions have approximately the same mobility[27].

EIS measurements were performed with amplitudes between 10 and 100 mV (rms) (Figure S1, Supplementary material) and open circuit potentials were recorded between each impedance measurement. For amplitudes smaller than 50 mV (rms) dispersion of points was observed in medium and low frequency regions, since the signal to noise ratio is small, therefore, not adequate. Consequently, the measurements were performed applying 100 mV (rms), between 1 × 10^6 Hz and 10^{-2} Hz, recording 10 points per frequency decade. All impedance diagrams were validated using Kramers-Kronig Transforms (KKT). All electrochemical measurements were performed at (25 ± 2) ºC.

3. Results and Discussion

3.1. Atomic Force Microscopy (AFM)

Figure 3 shows the topographic images of 3D AFM of the free membranes. From these images, agglomerates (or grains) are observed for all samples, although smaller agglomerates are seen in the image corresponding to the membranes before immersion in KCl.

AFM images allowed obtaining the parameters given in Table 1. The roughness of the membrane **A** increases with the immersion time, indicating changes in the membrane surface, while the membrane **B** shows no significant variation in roughness during all the immersion time (24 h), indicating that the membrane surface remains almost unchanged.

3.2. Raman spectroscopy

Figure 4 shows intensity Raman spectra for the membranes before and after immersion in 0.1 mol/L KCl for 24 h. The assignments of the bands were made according to previous studies on polyurethanes[28-33].

The bands detected in the Raman spectra were the same for all membranes, but different intensity can be seen to some

Figure 2. Double-compartment cell[25] used in the permeation tests and built in our laboratory[26].

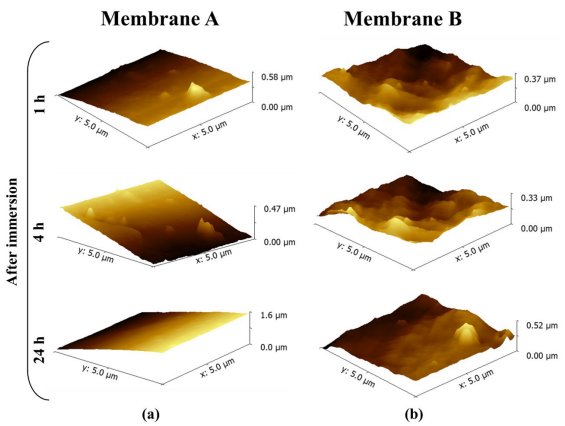

Figure 3. Topographic AFM images of (a) membrane **A** and (b) membrane **B**, obtained before and after 1, 4 and 24 h of immersion in 0.1 mol/L KCl, respectively.

Table 1. Roughness calculated from the AFM images of the membranes **A** and **B**.

Time of immersion (h)	Membrane A	Membrane B
	R_{RMS}/μm	
1	0.111	0.075
4	0.117	0.060
24	0.434	0.073

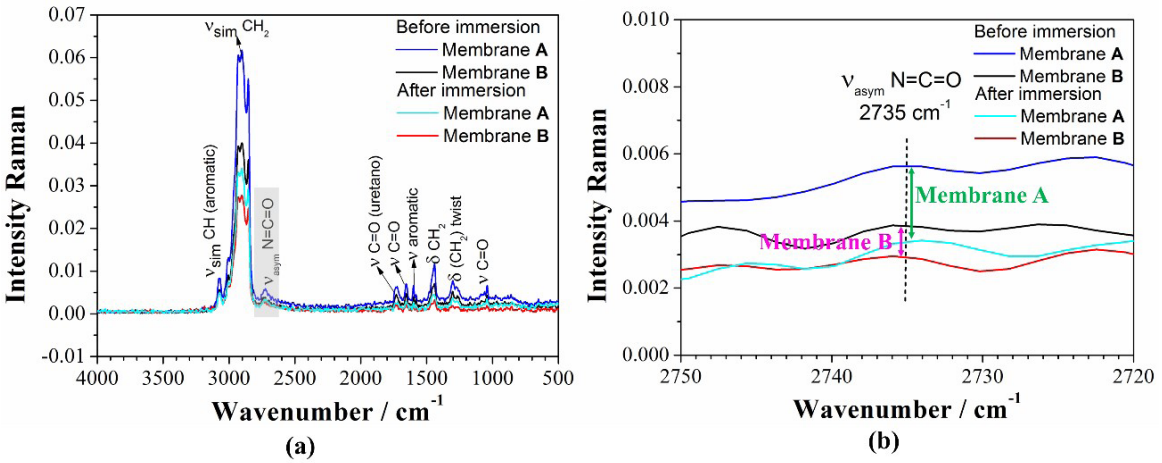

Figure 4. (a) Raman spectra obtained for membranes **A** and **B** before and after immersion in 0.1 mol/L KCl for 7 days and (b) zoom-in of the band for N=C=O group.

bands (Figure 4a). The most intense bands were observed at 2928 cm^{-1} and 2855 cm^{-1} both attributed to $\nu_{sim}(CH_2)$ vibration. The other bands occurred at: 3079 cm^{-1} assigned to ν_{sim}(CH) aromatic group; 2735 cm^{-1} to ν_{ass}(N=C=O) (Figure 4b); 1729 cm^{-1} to ν(C=O) urethane; 1659 cm^{-1} to ν(C=O) ester; 1600 cm^{-1} to ν(aromatic ring); 1438 cm^{-1} to $\delta(CH_2)$; 1295 cm^{-1} to $\delta(CH_2)$ – twist and at 1044 cm^{-1} the stretching of C=O[28]. There is no difference in the bands position before and after immersion in 0.1 mol/L KCl, but the intensity decreases, being more pronounced to the band attributed to the N=C=O group at ~2735 cm^{-1} (Figure 4b). The intensity decrease of this band was higher for membrane **A** than for Membrane **B** after 24 h of immersion, which may be associated with the consumption of NCO[34] to form biuret as illustrated in Figure 5. The greater amount of HDI in membrane **A** compared to **B**, i.e., more reactive functional NCO groups are present in **A** than in **B**, favored the reaction with water, resulting in higher electrolyte permeation through this polymeric matrix.

The formation of biuret group in the reaction of HDI with water[35,36] is, therefore, an important aspect in this study to interpret the decrease in the N=C=O band after 24 h of immersion. Therefore, a greater number of biuret groups is formed in membrane **A** than in **B**.

3.3. Electrochemical impedance spectroscopy (EIS) of the membrane in the permeation cell

Before the electrochemical study, the membrane thickness was determined. The average thickness of the membrane **A** is (491 ± 1) μm and membrane **B** is (328 ± 1) μm.

Figures 6 and 7 show the impedance diagrams for the membranes **A** and **B** obtained in KCl solution at different permeation times. At 0.01 Hz, the impedance value for membrane **A** is ~ 1.6×10^9 Ω cm^2 (Figure 6), while for membrane **B** (Figure 7) is ~ 1.2×10^9 Ω cm^2. Considering the different permeation times, the impedance values varied more for membrane **A** than **B**, which may be related to the interaction of the isocyanate groups with the water from the electrolyte.

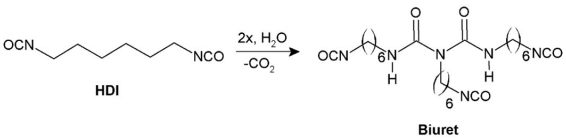

Figure 5. Isocyanate chemistry with hexamethylene diisocyanate (HDI)[23,35,36].

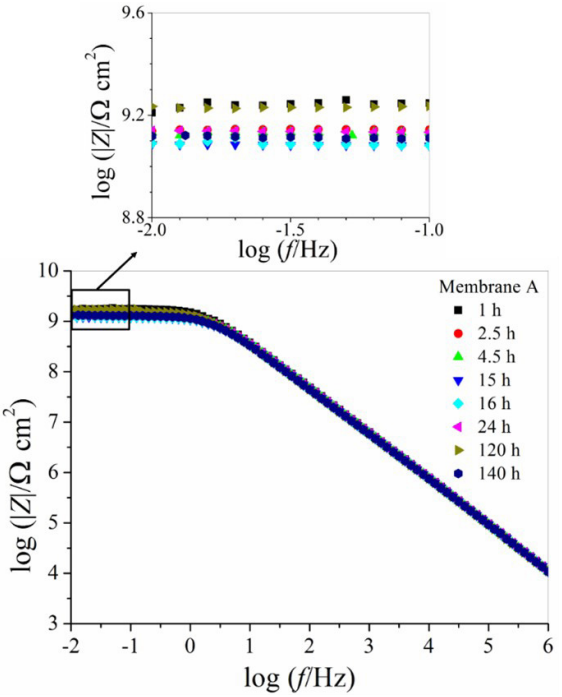

Figure 6. Impedance modulus |Z| Bode plots for the membrane **A** obtained in 0.1 mol/L KCl, with 100 mV (rms) amplitude in a permeation cell.

The changes in the impedance diagrams for the membrane **B** with time are not significant compared to those in membrane **A**, suggesting that there is no appreciable permeation of

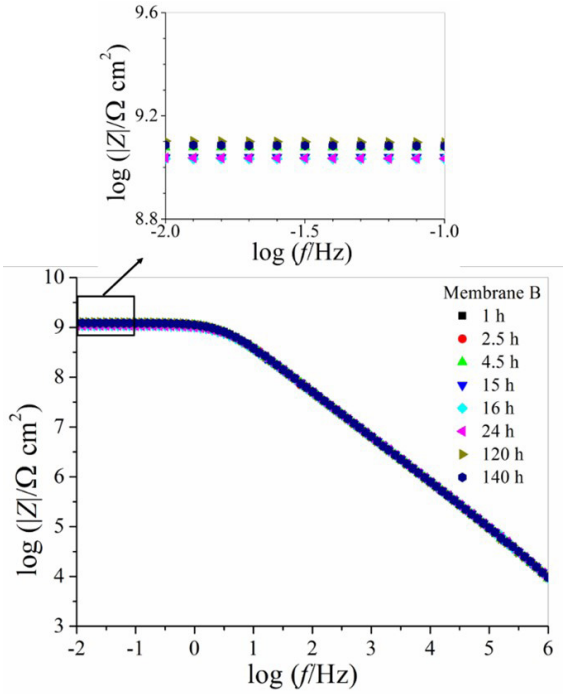

Figure 7. Impedance modulus |Z| Bode plots for the membrane **B** obtained in 0.1 mol/L KCl, with 100 mV (rms) amplitude and permeation cell.

the electrolyte and charge transfer through the membrane **B**. In case of membrane **A**, the $|Z|_{0.01Hz}$ value decreased 22.5% from 1 h to 140 h of permeation, while only ~1% was observed for membrane **B** (Figure S2). For the first 16 h, Figure S2 indicates greater rate of variation in $|Z|_{0.01Hz}$ values for membrane **A** than membrane **B**, suggesting that the greater amount of HDI in membrane **A** (functional NCO groups) favors the reaction with water, resulting in higher electrolyte permeation through this polymeric matrix. From 16 to 120 h the kinetic of permeation (variation of $|Z|_{0.01Hz}$ values with time) decreases for both membranes, attributed to the consumption / depletion of the NCO groups caused by the biuret reaction in both sides of the membranes. The $|Z|_{0.01Hz}$ values increased again at 140 h of immersion for both membranes **A** and B, however, much lower variation is observed for membrane **B**.

3.4. Charge transfer resistances (R_{CT}) and exchange current density (i_0)

Considering the complex plane response, reasonably well-defined semicircles were obtained for membranes **A** and **B** (Figure S3, Supplementary material), allowing easy determination of charge transfer resistance. The R_{CT} values obtained as illustrated in Figure S3 for both membranes are given in Table 2. The R_{CT} values systematically decrease until 16 h of permeation, then slightly increased up to 120 h and decreased again up to 140 h. As expected, the R_{CT} values showed the same tendency observed in Figure S2 (Supplementary material). So, the variation of the R_{CT} values is in line with the other analyses and causally related to the electrolyte permeation.

Table 2. Charge transfer resistances (R_{CT} /Ω cm²) and exchange current density (i_0 /A cm⁻²) for membranes **A** and **B**.

Time / h	Membrane A		Membrane B	
	$R_{CT}/10^9$ Ω cm²	$i_0/10^{-11}$ A cm⁻²	$R_{CT}/10^9$ Ω cm²	$i_0/10^{-11}$ A cm⁻²
1	1.75	1.46	1.20	2.12
2.5	1.38	1.85	1.19	2.14
4.5	1.33	1.92	1.18	2.16
15 h	1.20	2.12	1.08	2.36
16	1.21	2.11	1.07	2.38
24	1.36	1.87	1.07	2.38
120	1.53	1.67	1.25	2.04
140	1.27	2.01	1.24	2.05

In our case, we are considering that the resistance offered by the monolith to the electrolyte permeation can be measured as a resistance to the charge transport inside the membrane, since the ions needs to cross the solution / monolith interface and then propagates through the membrane. The determination of the R_{CT} and exchange current density (i_0) are relevant to characterize the barrier properties of the membrane. The i_0 reflects the rate that the salt ions can enter the membrane[4].

The relationship between R_{CT} and potassium ions concentration follows the Equation 1[19]. This is theoretically expected since the i_0 at a membrane / solution interface should follow the Equation 2.

$$R_{CT} \propto (C_{K^+})^{-\frac{1}{2}} \quad (1)$$

$$i_0 = nFk^0 (C_{K^+})^{\alpha} (\bar{C}_{K^+})^{1-\alpha} \quad (2)$$

where C_{K^+} is the concentration of K^+ in the aqueous phase, $\bar{C}_{K^+}$ the corresponding concentration in the membrane, k^0 is the heterogeneous rate constant for the charge exchange (transfer) process, whilst α is the transfer coefficient which is normally expected to be near 0.5[4,19]. The relationship between R_{CT} and i_0 when α is near 0.5 is given by Equation 3.

$$R_{CT} = \frac{RT}{nFi_0} \quad (3)$$

Equation 2 considers the fact that changing C_{K^+} changes both the interfacial potential difference according to Nernst equation and the rate of ions crossing the interface. According to Equation 3, the i_0 is inversely proportional to R_{CT} values as shown in Table 2.

For a direct comparison between the membranes **A** and **B**, the impedance results should be normalized for the membrane thickness, which is obtained dividing the $|Z|$ values by the corresponding membrane thickness, now given in Ω cm.

Figure 8 shows the impedance modulus Bode plots normalized for the thickness of the membranes. The graphs are represented on the same scale to better visualize the difference between the membranes. The membrane **B** is much more resistant to electrolyte permeation than membrane **A** (Figure 8). Figure 8 evidences the importance of considering the thickness of membranes to better interpret the EIS results of electrolyte permeation or membranes performance.

The normalized calculated R_{CT} to unitary thickness is summarized in Supplementary material (Table S1, Supplementary material) and represented in Figure 9a. Note that for membrane **A** R_{TC} values decrease with permeation time, while for membrane **B** R_{TC} values increase with permeation time. These results suggest a greater mobility of potassium ions within membrane **A** than in membrane **B**. Figure 9b shows the evolution of $|Z|_{0.01\ Hz}$ / thickness *vs.* time obtained from EIS data.

In the case of EIS analysis of barrier membranes or coatings, it is well known that failure is evidenced by the decrease of the low frequency impedance values[37]. It is evident from Figure 9b that the low frequency impedance / thickness of membrane **A** drops from 3.58×10^{10} Ω cm to 2.75×10^{10} Ω cm during 4.5 h of permeation, while for membrane **B** this parameter slight varied between 3.68×10^{10} Ω cm to 3.62×10^{10} Ω cm during 4.5 h of permeation, but it does not mean that the membranes failed, since the impedance increased for longer immersion times. The initial change indicates that solution enter in the membranes and the conductivity increased, mainly for membrane **A**, suggesting that the surface of both sides of the membrane **A** may have a more open structure than membrane **B**, in which the changes are less evident. At the end of the experiment (140 h), the impedance values at low frequency were 2.60×10^{10} Ω cm and 3.70×10^{10} Ω cm for membranes **A** and **B**, respectively. This implies that if the coating **B** has the same thickness of coating **A**, it may present better barrier property than coating

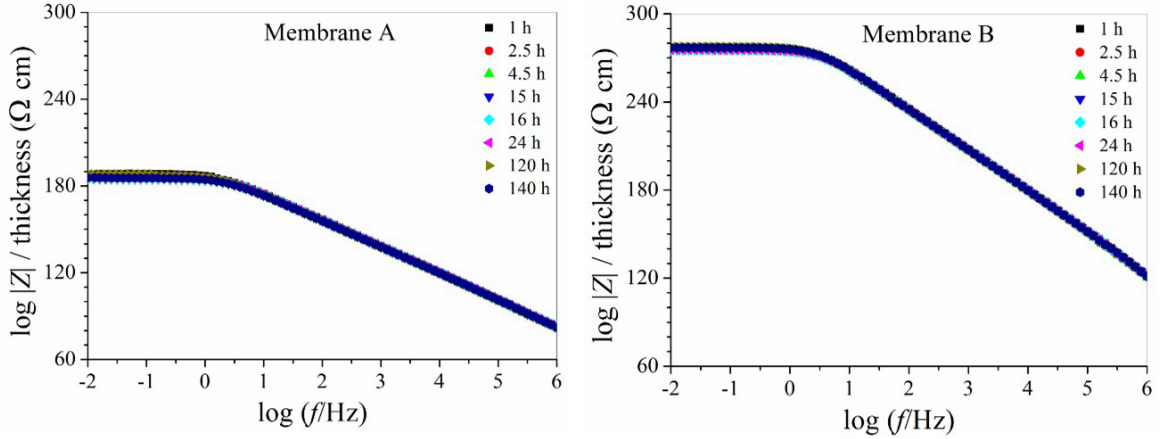

Figure 8. Impedance modulus |*Z*| / thickness *versus* frequency for membrane **A** and membrane **B**.

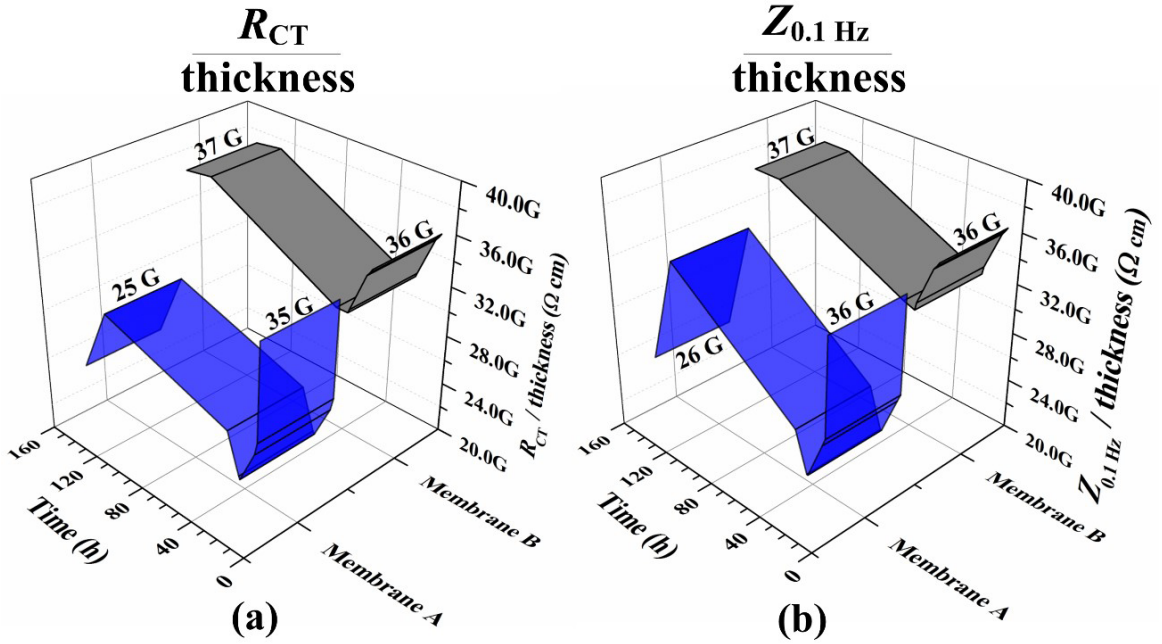

Figure 9. Normalized **(a)** R_{CT} and **(b)** $|Z|_{0.01Hz}$ values for membranes thickness as a function of exposure time in 0.1 mol/L KCl. Blue color corresponds to membrane **A**.

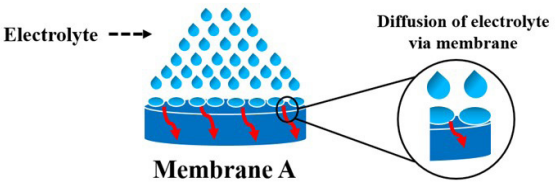

Figure 10. Schematic representation of the electrolyte permeation in membrane **A**.

A when applied on a metallic surface, and the decrease of impedance at low frequency for coating **A** could also indicate higher probability of failing. The better performance of coating **B** against corrosion of aluminum alloy (AA 1200) in 3.5% NaCl aerated solution was already demonstrated[1]. The results indicated greater corrosion resistance for coating **B** in the presence and absence of inhibitors in solution.

Hence, the barrier protection performance of the two membranes can be placed in the following increasing order: membrane **A** < membrane **B**. Figure 10 shows a schematic representation of the electrolyte permeation in membrane **A**. At the initial, the permeation is facilitated due to the reaction of the NCO group with water leading to the formation of biuret (Figure 5), therefore, membrane **A** that has more HDI in its formulation reacts with more water, thus the electrolyte permeation and water uptake are higher in relation to membrane **B**. In comparison to membrane **B**, the membrane **A** facilitates the penetration of water and consequently of K^+ ions.

In addition to the membrane formulation, whose barrier properties can be evaluated according to the methodology described in the present work, to have membranes with good performance against corrosion it is extremely important the surface preparation of the substrate and uniform membrane / coating deposition to avoid the formation of defects during this process, which may lead the membrane or coating to fail.

4. Conclusion

Organic-base membranes prepared with crambe and castor oils and with roughness (R_{RMS}) from 0.060 to 0.434 µm and thickness between 328 and 491 µm were tested for ions permeability in 0.1 mol/L KCl aqueous solution. Raman spectroscopic studies allowed identifying the functional groups, assigning the main vibrations of the free membranes, and indicating the formation of biuret groups when in contact with aqueous solution.

Both membranes have low ions permeability, but membrane **B** presented less variation of R_{TC} and i_0 values with the testing time than membrane **A**. The normalized R_{TC} and $|Z|_{0.01Hz}$ values for the membrane thickness, at the same conditions, indicated that membrane **B** presents higher barrier properties, which can lead to a higher protection performance of metallic surfaces against corrosion compared to membrane **A**.

This study may serve as guide to a previous evaluation of organic resins, organic-inorganic hybrids monoliths, and some inorganic resins developed to be applied as coatings to protect metal surfaces against corrosion from aggressive solutions. The assessment of R_{RMS}, $R_{TC,}$ i_0 and $|Z|_{0.01Hz}$ parameters and, therefore, of barrier properties and even self-healing ability before resins application on surfaces can avoid time loss and materials consume.

5. Acknowledgements

J.V. Nardeli author thanks the São Paulo state agency FAPESP (Process: 2015/10554-9 and 2018/09040-9) for scholarships.

6. References

1. Nardeli JV, Fugivara CS, Taryba M, Pinto ERP, Montemor MF, Benedetti AV. Tannin: a natural corrosion inhibitor for bare and coated aluminum alloys. Prog Org Coat. 2019;135:368-81. http://dx.doi.org/10.1016/j.porgcoat.2019.05.035.
2. Nardeli JV, Fugivara CS, Benedetti AV. Environmentally friendly coatings applied on aluminum alloy ASTM 1200. In: 64th Annual Meeting of the International Society of Electrochemistry; 2013; Santiago de Querétaro. Proceedings. Switzerland: International Society of Electrochemistry; 2013. p. 1-184.
3. Nardeli JV, Snihirova DV, Fugivara CS, Montemor MF, Pinto ERP, Messaddecq Y, et al.. Localised corrosion assessement of Crambe-oil-based polyurethane coatings applied on the ASTM 1200 aluminum alloy. Corros Sci. 2016;111:422-35. http://dx.doi.org/10.1016/j.corsci.2016.05.034.
4. Aramaki K. Self-healing mechanism of an organosiloxane polymer film containing sodium silicate and cerium(III) nitrate for corrosion of scratched zinc surface in 0.5 M NaCl. Corros Sci. 2002;44(7):1621-32. http://dx.doi.org/10.1016/S0010-938X(01)00171-8.
5. Ammar S, Iling AWM, Ramesh K, Ramesh S. Development of fully organic coating system modified with epoxidized soybean oil with superior corrosion protection performance. Prog Org Coat. 2020;140:105523. http://dx.doi.org/10.1016/j.porgcoat.2019.105523.
6. Nardeli JV, Fugivara CS, Taryba M, Montemor MF, Ribeiro SJL, Benedetti AV. Novel healing coatings based on natural-derived polyurethane modified with tannins for corrosion protection of AA2024-T3. Corros Sci. 2020;162:108213. http://dx.doi.org/10.1016/j.corsci.2019.108213.
7. Li X, Bandyopadhyay P, Nguyen TT, Park O, Lee JH. Fabrication of functionalized graphene oxide/maleic anhydride grafted polypropylene composite film with excellent gas barrier and anticorrosion properties. J Membr Sci. 2018;547:80-92. http://dx.doi.org/10.1016/j.memsci.2017.10.031.
8. Bandyopadhyay P, Park WB, Layek RK, Uddin ME, Kim NH, Kim H, et al. Hexylamine functionalized reduced graphene oxide/polyurethane nanocomposite-coated nylon for enhanced hydrogen gas barrier film. J Membr Sci. 2016;500:106-14. http://dx.doi.org/10.1016/j.memsci.2015.11.029.
9. Dong Y, Feng X, Dong D, Wang S, Yang J, Gao J, et al. Elaboration and chemical corrosion resistance of tubular macro-porous cordierite ceramic membrane supports. J Membr Sci. 2007;304(1-2):65-75. http://dx.doi.org/10.1016/j.memsci.2007.06.058.
10. Nardeli JV, Fugivara CS, Taryba M, Montemor MF, Benedetti AV. Biobased self-healing polyurethane coating with Zn micro-flakes for corrosion protection of AA7475. Chem Eng J. 2021;404:126478. http://dx.doi.org/10.1016/j.cej.2020.126478.
11. Nardeli JV, Fugivara CS, Taryba M, Montemor MF, Benedetti AV. Self-healing ability based on hydrogen bonds in organic coatings for corrosion protection of AA1200. Corros Sci. 2020;177:108984. http://dx.doi.org/10.1016/j.corsci.2020.108984.
12. Cañas A, Ariza MJ, Benavente J. Characterization of active and porous sublayers of a composite reverse osmosis membrane by impedance spectroscopy, streaming and membrane potentials, salt diffusion and X-ray photoelectron spectroscopy measurements.

J Membr Sci. 2001;183(1):135-46. http://dx.doi.org/10.1016/S0376-7388(00)00583-4.

13. Efligenir A, Fievet P, Deon S, Salut R. Characterization of the isolated active layer of a NF membrane by electrochemical impedance spectroscopy. J Membr Sci. 2015;477:172-82. http://dx.doi.org/10.1016/j.memsci.2014.12.044.
14. Gao F, Wang J, Zhang HW, Jia H, Cui Z, Yang G. Role of ionic strength on protein fouling during ultrafiltration by synchronized UV-vis spectroscopy and electrochemical impedance spectroscopy. J Membr Sci. 2018;563:592-601. http://dx.doi.org/10.1016/j.memsci.2018.06.030.
15. Jing Y, Chaplin BP. Electrochemical impedance spectroscopy study of membrane fouling characterization at a conductive sub-stoichiometric TiO_2 reactive electrochemical membrane: transmission line model development. J Membr Sci. 2016;511:238-49. http://dx.doi.org/10.1016/j.memsci.2016.03.032.
16. DuToit M, Ngaboyamahina E, Wiesner M. Pairing electrochemical impedance spectroscopy with conducting membranes for the in situ characterization of membrane fouling. J Membr Sci. 2021;618:118680. http://dx.doi.org/10.1016/j.memsci.2020.118680.
17. Fortunato R, Branco LC, Afonso CAM, Benavente J, Crespo JG. Electrical impedance spectroscopy characterisation of supported ionic liquid membranes. J Membr Sci. 2006;270(1-2):42-9. http://dx.doi.org/10.1016/j.memsci.2005.06.040.
18. Armstrong RD, Covington AK, Evans GP. Mechanistic studies of the valinomycin-based potassium-selective electrode using ac impedance. J Electroanal Chem. 1983;159(1):33-40. http://dx.doi.org/10.1016/S0022-0728(83)80312-X.
19. Armstrong RD, Lockhart JC, Todd M. The mechanism of transfer of K^+ between aqueous solutions and PVC membranes containing valinomycin. Electrochim Acta. 1986;31(5):591-4. http://dx.doi.org/10.1016/0013-4686(86)85038-1.
20. Armstrong RD, Nikitas P. Transport of K^+ in PVC matrix membranes containing valinomycin. Electrochim Acta. 1985;30(12):1627-9. http://dx.doi.org/10.1016/0013-4686(85)87008-0.
21. Margarit ICP, Mattos OR. About coatings and cathodic protection: properties of coatings influencing delamination and cathodic protection criteria. Electrochim Acta. 1998;44(2-3):363-71. http://dx.doi.org/10.1016/S0013-4686(97)10193-1.
22. Castela ASL, Simões AM, Ferreira MGS. EIS evaluation of attached and free polymer films. Prog Org Coat. 2000;38(1):1-7. http://dx.doi.org/10.1016/S0300-9440(99)00076-4.
23. Nardeli JV, Fugivara CS, Pinto ERP, Polito WL, Messaddeq Y, Ribeiro SJL, et al. Preparation of polyurethane monolithic resins and modification with a condensed tannin-yielding self-healing property. Polymers (Basel). 2019;11(11):1890. http://dx.doi.org/10.3390/polym11111890.
24. Nardeli JV, Fugivara CS, Montemor MF, Benedetti AV. Smart coating for corrosion protection of aluminium alloys: global and localized study of anti-corrosion performance. In: Nardeli JV, editor. A diversidade de debates na pesquisa em química 2. Ponta Grossa: Atena; 2020. p. 1-12. http://dx.doi.org/10.22533/at.ed.3602021051.
25. Devanathan MAV, Stachurski Z, Beck W. A technique for the evaluation of hydrogen embrittlement characteristics of electroplating baths. J Electrochem Soc. 1963;110(8):886-90. http://dx.doi.org/10.1149/1.2425894.
26. Modiano S, Carreno JAV, Fugivara CS, Torresi RM, Vivier V, Benedetti AV, et al. Changes on iron electrode surface during hydrogen permeation in borate buffer solution. Electrochim Acta. 2008;53(10):3670-9. http://dx.doi.org/10.1016/j.electacta.2007.11.077.
27. Duarte AR, Batalioto F, Barbero G, Figueiredo AM No. Measurement of the impedance of aqueous solutions of KCl: an analysis using an extension of the Poisson-Nernst-Planck model. Appl Phys Lett. 2014;105(2):022901. http://dx.doi.org/10.1063/1.4890386.
28. Miller CE, Archibald DD, Myrick ML, Angel SM. Determination of physical properties of reaction-injection-molded polyurethanes by NIR-FT-Raman spectroscopy. Appl Spectrosc. 1990;44(8):1297-300. http://dx.doi.org/10.1366/000370290789619577.
29. Romanova V, Begishev V, Karmanov V, Kondyurin A, Maitz MF. Fourier transform Raman and Fourier transform infrared spectra of cross-linked polyurethaneurea films synthesized from solutions. J Raman Spectrosc. 2002;33(10):769-77. http://dx.doi.org/10.1002/jrs.914.
30. Janik H, Palys B, Petrovic ZS. Multiphase-separated polyurethanes studied by micro-raman spectroscopy. Macromol Rapid Commun. 2003;24(3):265-8. http://dx.doi.org/10.1002/marc.200390039.
31. Parnell S, Min K, Cakmak M. Kinetic studies of polyurethane polymerization with Raman spectroscopy. Polymer (Guildf). 2003;44(18):5137-44. http://dx.doi.org/10.1016/S0032-3861(03)00468-3.
32. Weakley AT, Warwick PCT, Bitterwolf TE, Aston DE. Multivariate analysis of micro-raman spectra of thermoplastic polyurethane blends using principal component analysis and principal component regression. Appl Spectrosc. 2012;66(11):1269-78. http://dx.doi.org/10.1366/12-06588.
33. Bruckmoser K, Resch K. Investigation of ageing mechanisms in thermoplastic polyurethanes by means of IR and Raman spectroscopy. Macromol Symp. 2014;339(1):70-83. http://dx.doi.org/10.1002/masy.201300140.
34. Morsch S, Lyon S, Greensmith P, Smith SD, Gibbon SR. Water transport in an epoxy–phenolic coating. Prog Org Coat. 2015;78:293-9. http://dx.doi.org/10.1016/j.porgcoat.2014.08.006.
35. Golling FE, Pires R, Hecking A, Weikard J, Richter F, Danielmeier K, et al. Polyurethanes for coatings and adhesives: chemistry and applications.. Polym Int. 2019;68(5):848-55. http://dx.doi.org/10.1002/pi.5665.
36. Shkapenko G, Gmitter GT, Gruber EE. Mechanism of the Water-lsocyanate Reaction. Ind Eng Chem. 1960;52(7):605-8. http://dx.doi.org/10.1021/ie50607a031.
37. Shreepathi S, Naik SM, Vattipalli MR. Water transportation through organic coatings correlation between electrochemical impedance measurements, gravimetry, and water vapor permeability. J Coat Technol Res. 2012;9(4):411-22. http://dx.doi.org/10.1007/s11998-011-9376-4.

Supplementary material

The following online material is available for this article:

Figure S1 - Complex plane plots obtained for membrane B at different amplitudes between 10 mV(rms) and 100 mV(rms), in 0.1 mol L^{-1} KCl solution, at 25 oC.

Figure S2 - Evolution of the impedance modulus at 0.01 Hz for membranes A and B immersed in 0.1 mol L^{-1} KCl.

Figure S3 - Nyquist plots for membranes A and B in 0.1 mol L^{-1} KCl solution.

Table S1 - Normalized charge transfer resistances (RCT/Ω cm) for the thickness of membranes A and B.

This material is available as part of the online article from https://doi.org/10.1590/1980-5373-MR-2022-0129